# Comparison of measured poloidal rotation in MAST spherical tokamak plasmas with neo-classical predictions

A. R. Field[1], J. McCone[2], N. J. Conway[1], M. Dunstan[1], S. Newton[1] and M. Wisse[1]

[1] EURATOM/UKAEA Fusion Association, Culham Science Centre, Oxon, OX14 3DB, UK

[2] Department of Physics, University College Cork, Association EURATOM-DCU Ireland.

* Electronic Mail Address: anthony.field@ukaea.org.uk

## Abstract

Neo-classical tokamak plasma theory predicts poloidal rotation driven by the temperature gradient of order ~ few km/s. In conventional aspect ratio tokamak plasmas, e.g. on JET and DIII-D, poloidal velocities considerably in excess of the neo-classical values have been measured, particularly in the presence of internal transport barriers (ITBs), by means of charge-exchange recombination spectroscopy (CXRS) on the fully ionised $C^{6+}$ impurity ions. Comparison between such measurements and theoretical predictions requires careful corrections to be made for apparent 'pseudo' velocities, which can arise from the finite lifetime of the excited atoms in the magnetised plasma and the energy dependence of the charge-exchange excitation process. In present day spherical tokamak (ST) plasmas this correction is an order of magnitude smaller than on large conventional tokamaks, which operate at higher temperature and magnetic field, hence reducing any associated systematic uncertainties. On MAST measurements of toroidal and poloidal flows of the $C^{6+}$ impurities are available from high-resolution Doppler CXRS measurements, where the appropriate corrections for the pseudo-velocities are made. Comparison of the measured $C^{6+}$ velocities with neo-classical theory requires calculation of the impurity flow, which differs from that of the bulk ions due to the respective diamagnetic contributions for each species and inter-species friction forces. Comparisons are made with the predictions of a recent neo-classical theory [1, 2], which calculates the full neo-classical transport matrix for bulk ions and a single impurity species for a strongly rotating plasma, as well as a simpler neo-classical theory [3] for an impure plasma. Initial results for both L- and H-mode plasmas show that, within the measurement uncertainties, the measured poloidal rotation of the core plasma is consistent with the neo-classical predictions.

## 1 Introduction

It is important to understand the driving and damping mechanisms of poloidal rotation as it plays a role in determining the radial electric field, which is known to suppress turbulence and thus improve confinement. It is also of interest because the driving mechanisms are more subtle than the relatively straightforward process of momentum transfer from the heating beams to the plasma, involving thermal forces as in the standard neo-classical theory [4] or perhaps the turbulent Reynold's stress [5]. The latter results from a finite temporal average of the correlation of fluctuating radial and poloidal velocities $\langle v_r v_\theta \rangle$, which can drive a mean poloidal flow if there is a radial gradient in this stress. Poloidal velocities well in excess of those predicted from neoclassical theory have been detected in H- and QH-mode plasmas in DIII-D [6], in the region of internal transport barriers in JET [7] and spontaneous reversals in poloidal flow were also observed on TFTR [8]. In contrast, preliminary measurements on the NSTX ST device of $C^{6+}$ poloidal velocity profiles are consistent with the predictions of neo-classical theory [9]. Various theories have been composed to account for this and Staebler [10] among others has suggested a turbulent drive for these flows associated with drift waves. The JET results have been shown to be consistent with the mean poloidal flows being driven by the Reynolds stress by means of comparisons with results from numerical turbulence simulations [11].

The main aim of this paper is to investigate whether the poloidal velocities observed in MAST spherical tokamak plasmas are consistent with predictions of neo-classical theory or whether similar discrepancies are observed as on conventional-aspect ratio devices. There are several advantages in making such a comparison on MAST. Firstly, the CXRS velocity measurements available on MAST [12] have a very high spatial resolution $\Delta R$ of about 1 cm, which is of the same order as the ion Larmor radius $\rho_i$. Secondly, the poloidal lines of sight are also aligned to look directly downward so as not to pick up a component of the much larger toroidal flow, where typically $v_\phi / v_\theta \sim$ 10-100. Finally, due to its low magnetic field ($B_t \sim 0.6$ T) and relatively low temperature ($T_i \sim$ 1-2 keV), atomic physics corrections to the spectroscopic velocity measurements, which are

discussed below, are considerably smaller than is the case in conventional tokamaks making the comparison less prone to systematic errors.

In Sec. 2 a brief overview is given of the neo-classical theory of poloidal rotation, Sec. 3 discusses the pseudo-velocities which may arise when making spectroscopic Doppler velocity measurements on the line emission from ions of a magnetised plasma and the magnitudes of these corrections are estimated for typical MAST parameters. In Sec. 4 the results of a comparison between velocity profiles calculated using expressions from the two neo-classical theories [2, 3] are presented and in Sec. 5 the observed velocity profiles measured using the CXRS system are compared with these predictions. Finally, the conclusions that can be drawn from both comparisons are discussed.

## 2 Neo-classical Poloidal Rotation

Neo-classical theory [3] predicts poloidal rotation velocities of order $V_\theta^i \sim v_{thi}\rho_i / L_{T_i}$ to be driven by the ion temperature gradient even in a pure plasma, where $L_T$ is the ion temperature gradient scale length (defined as $L_T = T_i / T_i'$, where the prime denotes the radial gradient), $\rho_i$ is the Larmor radius of the bulk ions and $v_{thi} = \sqrt{2T_i / m_i}$ is the bulk ion thermal velocity. Note that because $V_\theta^i \propto T_i / B$, although $T_i \sim 10$ keV on large conventional tokamaks compared to ~ 1 keV in MAST plasmas, the much lower toroidal field on spherical tokamaks results in similar magnitudes for the predicted neo-classical velocities. For example, on DIII-D [6] predictions for $V_\theta^i$ using NCLASS gave values of magnitude < 2 km/s for plasmas with toroidal velocities approaching 600 km/s. In comparison, on MAST typical values of poloidal velocities are ~ 5-10 km/s with toroidal velocities of 100-200 km/s in the plasma core.

The neo-classical toroidal and poloidal rotation for the simplified case of bulk ions and a single impurity species is considered in Ref. 3, which gives an expression for the poloidal rotation velocity of the bulk ions $V_\theta^i$ as:

$$V_\theta^i = \frac{1}{2}\frac{v_{th,i}\rho_i}{L_{T_i}} K_1 \frac{BB_\phi}{\langle B^2 \rangle} \qquad (1)$$

where $K_1$ is a numerical factor of O(1), which is dependent upon the collisionality $\nu_i^*$ (defined as the relative magnitude of the ion-ion collision frequency $\nu_{ii}$ to the ion transit frequency $\nu_{th,i}/qR$), the impurity concentration quantified in terms of the impurity strength $\alpha = n_I Z_I^2 / n_i Z_i^2$ and the fraction of trapped particles. Here, $B$ is the magnitude of the total magnetic field, $B_\phi$ is the toroidal field component and $\langle B^2 \rangle$ is the flux surface average of $B^2$.

For the case of a single impurity species, the impurity poloidal velocity component $V_\theta^I$ is given by the expression:

$$V_\theta^I = \frac{1}{2}\frac{v_{th,i}\rho_i}{L_{T_i}}\left[\left(K_1 + \frac{3K_2}{2}\right)\frac{1}{L_{T_i}} - \frac{1}{L_{P_i}} + \frac{Z_i T_I}{Z_I T_i}\frac{1}{L_{P_I}}\right]\frac{BB_\phi}{\langle B^2 \rangle} \qquad (2)$$

where the terms in $1/L_{P_i}$ and $1/L_{PI}$ are diamagnetic corrections and $K_2$ is again a numerical factor of O(1) which is a different function of the same parameters as $K_1$. Calculations of $V_\theta^I$ are required for MAST parameters for comparison with poloidal velocities measured from the Doppler shift of impurity line emission.

Eqs. 1 and 2 are valid in all collisionality regimes but do not take into account the influence of any strong toroidal rotation, which can alter the poloidal distribution of the ions due to centrifugal forces and also drive fluxes and poloidal flow through any shear in the toroidal flow. The neo-classical theory has recently been extended to the case of a highly-rotating, impure plasma by Newton and Helander [2]. An expression for the poloidal velocity component of an ion species $s$ given in an extension of this work [1] as:

$$V_\theta^s = I\frac{T_i}{e}\frac{B_\theta}{\langle B^2 \rangle}\left(\frac{V_{1s}}{L_{T_i}} + \frac{V_{2s}}{L_{P_i}} + \frac{V_{3s}}{L_\omega}\right) \qquad (3)$$

Here $I = RB_\phi$ where $R$ is the major radius, $B_\theta$ is the poloidal magnetic field component and $L_\omega$ is the scale length of the toroidal angular velocity $\omega$. Expressions for the coefficients $V_{1s}$, $V_{2s}$ and $V_{3s}$ are given in Ref. 1. The poloidal velocities of either the bulk ions or impurities can be obtained from this expression with the appropriate substitution of $s$ for $i$ or $I$. This expression is valid for a low-collisionality bulk plasma with the

impurities in the collisional regime. With fully ionised carbon as the dominant impurity and deuterium bulk ions, as is typically the case on MAST, sheared toroidal rotation is not predicted to drive poloidal flow. This is because in the third term on the RHS of equation Eq. 3 the coefficient $V_{3s} \propto M_{i0}^2 - M_{z0}^2/z$ (where the square of the toroidal Mach number $M_{s0}^2 = m_s R^2 \omega^2 / 2T_i$ ) is identically zero if the charge to mass ratio of the bulk ions and impurities are equal. In this case, neglecting the influence of sheared rotation is therefore not a serious deficiency in the work of Ref. 3.

**3 Atomic Physics Corrections**

A local measurement of the fluid velocity of impurity ions in a magnetised plasma can be determined from the Doppler shift of line emission excited by charge exchange between the energetic injected beam atoms and the ionised impurities,

$$D^0(n_D) + A^{z+} \rightarrow D^+ + A^{(z-1)+}(n)^* \qquad (4)$$

where $A^{z+}$ is the recipient ion, $z$ is the charge state before charge exchange, $n$ is the excited state after charge-exchange and $n_D$ is the energy state of the beam neutral. The measurements presented here use the $C^{5+}$ (n=8→7) transition at 529.05 nm wavelength. The atomic physics processes governing the excitation and decay of the observed transition can themselves lead to an apparent Doppler shift of the line profile, even in the absence of any fluid rotation. These so-called 'pseudo' velocities can be significant and careful analysis is required if meaningful comparisons between measurements and theoretical predictions are to be made.

The line intensity, $I \propto n_b n_s \sigma_{cx}^k |\mathbf{V} - \mathbf{V}_b|$, where $n_b$ is the density of the beam ions $n_s$ is the density of the ground state impurity ions, $\sigma_{cx}^k$ is the charge exchange cross-section for excited state $k$ and $|\mathbf{V} - \mathbf{V}_b|$ is the relative velocity between the beam atoms and the recipient ions. The charge-exchange cross-section is strongly energy dependent $\sigma_{cx}^k(E_{rel}) = \sigma_{cx}^k(m_i |\mathbf{V} - \mathbf{V}_b|^2/2)$ and this in itself can lead to an apparent velocity shift. When the thermal velocity $v_{thi}$ is significant compared to the beam velocity, $v_b = \sqrt{2eE_b / m}_b$ the cross-section for ions moving towards the beam can differ from that for ions moving away from the beam on opposite sides of the Larmor orbit. This will

enhance the observed intensity on one side of the line profile and diminish it on the other leading to an apparent line shift, equivalent to a pseudo-velocity $\Delta v_{cx}^{*}$. Although one would expect this shift to be largest when observing along the beam, an apparent line shift may also be observed when viewing perpendicular to the beam if the lifetime of the excited state $\tau_k$ is significant compared with the gyro-period, i.e. $\omega_s \tau_k \sim \mathrm{O}(1)$, where $\omega_s$ is the gyro-frequency. This is because the gyro-motion of the excited ions results in a velocity component in the direction perpendicular to the beam.

The magnitude of this apparent velocity can be estimated from the following simplified expression:

$$\Delta v_{cx}^{*} = \frac{v_{thi}^2}{2c}\sqrt{2E_b m_i}\,\frac{1}{\sigma_{cx}^{k}}\frac{d\sigma_{cx}^{k}}{dE_b}\frac{1}{1+(\omega_s\tau_k)^2}(\omega_s\tau_k + \cos\alpha) \qquad (5)$$

where $c$ is the speed of light and $\alpha$ is the angle between the line-of-sight and the beam in the plane of the Larmor orbit. When viewing perpendicular to the beam ($\alpha = \pi/2$) and if $(\omega_s\tau_k)^2 << 1$ this velocity shift scales as $T_I B$. Hence, these corrections are much larger for measurements made on large, conventional aspect-ratio tokamaks, which typically operate at much higher temperature and magnetic field than do current spherical tokamaks.

This effect has been considered in greater detail in earlier work on TFTR [13] and later on DIII-D [6]. In particular, the influence of charge exchange from the $E_b/2$ and $E_b/3$ components of the beam, which will have a different energy dependence of $\sigma_{cx}^{k}$ and also of charge exchange from excited states of the beam atoms, e.g. $n_D = 2$, which can have an opposite sign of $d\sigma_{cx}^{k}/dE_b$ from that of the ground state, are considered. Expressions equivalent to Eq. 5 are also given for a general beam and viewing geometry, where in [6] the effect of the finite lifetime is conveniently handled as a vector operator on the velocity vector.

The lifetime of the excited n=8 state $\tau_k$ can differ from that due to spontaneous decay ($\tau_k = 1/A_{jk} = 0.54$ ns) due to collisional processes and an accurate value should be determined experimentally. In Ref. [13] this parameter is determined from differences between measurements along up/down symmetric views at large angles ($\alpha \sim \pm\pi/4$) to the mid-plane. In this case the lifetime is given by:

$$\tau_k = \frac{v_{app}^{+} - v_{app}^{-}}{v_{app}^{+} + v_{app}^{-}} \frac{\tan\alpha}{\omega_s} \tag{6}$$

where $v_{app}^{+}$ and $v_{app}^{-}$ are the apparent velocities measured along the upper and lower views respectively. In this work a value of 1.1 ns was determined which is longer than the radiative lifetime of 0.54 ns. This could be explained if incomplete statistical mixing of the *l*-levels within the n=8 level was assumed in a collisional radiative model.

The likely magnitude of this pseudo-velocity $\Delta v_{cx}^{*}$ can be estimated from Eq. 5 assuming typical MAST core plasma parameters of $T_i$ = 1 keV and $B_t$ = 0.5 T with a 50 keV deuterium beam. Assuming the value for $\tau_k$ of 1.1 ns determined in Ref. 13 results in a value $\omega_s \tau_k \sim 0.022$, i.e. about 2% of the apparent velocity that would be observed looking along the beam would be observed when viewing vertically.

An estimate of the energy dependence $\left(d\sigma_{cx}^{k}/dE_b\right)/\sigma_{cx}^{k}$ for the full-energy component of a 50 keV deuterium beam of $10^{-4}$ $eV^{-1}$ is obtained from ADAS [14] atomic data. Using this value the estimated apparent velocity $\Delta v_{cx}^{*}(\alpha = 0)$ when viewing along the beam would be 38 km/s towards the observer, which is certainly significant even compared to the observed toroidal velocities of typically 100-200 km/s. Due to the small value of $\omega_s \tau_k \sim 0.022$, however, the apparent poloidal velocity when observing vertically $\Delta v_{cx}^{*}(\alpha = \pi/2) \sim 0.8$ km/s is much smaller.

A further effect that can lead to an apparent velocity is that due to a gradient in the excitation probability, e.g. due to a gradient in neutral beam density [15]. This effect is important where the scale length of the excitation rate $L_{\xi_k}$ is short in comparison to the gyro-radius $\rho_s$, as is the case for measurements based on passive line emission in the pedestal region of an H-mode plasma where the electron density gradient scale length can be of the order of the ion Larmor radius.

The apparent velocity due to this effect $\Delta v_{ex}^{*}$ can be estimated from:

$$\Delta v_{ex}^{*} = -\frac{1}{2} v_{ths} \frac{\rho_s}{L_{\xi_k}} \frac{(\omega_s \tau_k)^2}{1 + (\omega_s \tau_k)^2} \tag{7}$$

where $\xi_k$ is the excitation probability, $\omega_s$ is the gyro-frequency of the ion $s$ in the magnetic field and $\tau_k$ is the life time of the excited state of the observed transition. The origin of this effect is similar to that of the diamagnetic velocity in that the gradient of the excitation rate will lead to a higher number of excited ions on one side of the Larmor orbit than the other. In the case of charge-exchange excitation with the beam the scale length of the excitation rate is of the order of the minor radius $L_\xi \sim a \sim 0.5$ m. For the parameters given above $\rho_s/L_\xi \sim 1.3\times10^{-2}$ and $v_{ths} \sim 1.3\times10^5$ m/s for the $C^{5+}$ ions giving a negligible apparent velocity from this effect of $\Delta v_{ex}^* \sim 0.4$ m/s.

**4 Predicted neo-classical poloidal velocities**

Here, the neo-classical poloidal velocities of the bulk ions and the carbon impurities calculated using the appropriate expressions from the theories of Kim [3] and Newton and Helander [1, 2] are compared. Ion temperatures and toroidal flow velocities of carbon ions are obtained from the CXRS measurements and equal bulk and impurity ion temperatures and toroidal velocities are assumed. (The validity of the latter assumption is unimportant as velocity shear does not enter into Eqs. 1 and 2 and the coefficient $V_{s3}$ in Eq. (3) is identically zero for equal bulk ion and impurity charge/mass ratio.) The electron density profile is obtained from Thomson scattering measurements, either from the multi-time point Nd:YAG system or from the high-spatial resolution Ruby system [16], the latter available at the NBI cut-off time for these discharges. Bulk ion and impurity density profiles are calculated from the electron density and measured $Z_{eff}$ profile, which is determined from 2D imaging of the visible bremsstrahlung emission [17], by assuming that $C^{6+}$ is the dominant impurity. Finally, the magnetic data required to calculate the appropriate flux-surface averaged quantities in the theoretical expressions are obtained from an EFIT equilibrium reconstruction [18].

An example of the calculated poloidal velocities is shown in Fig. 1 for a sawtooth-free, L-mode plasma (#12546) with 800 kA plasma current, $B_t \sim 0.58$ T, line-average density $\bar{n}_e \sim 3\times10^{19}$ $m^{-3}$ and with 1.8 MW of co-injected, tangential NBI heating, where a positive $v_\theta$ corresponds to the ion diamagnetic direction. In this case, $Z_{eff} \sim 1.5$ in the core plasma increasing from $R \sim 1.2$ m outwards towards the plasma boundary. In the core plasma the bulk ion collisionality is low ($0.01 < \nu_i^* < 1$), exceeding unity only in the

plasma periphery ($r/a$ > 0.95) and the corresponding values of the coefficients in Eqs. 1 and 2 are $K_1 \sim 0.5$ and $K_2 \sim 0.6$ at $\varepsilon$ (= $r/R$) of 0.3.

The magnitudes of the velocities calculated according to Kim's theory are somewhat larger than those calculated from Newton's, with peak values in the gradient region at half-radius of ~ 5 km/s in the ion diamagnetic direction. The bulk ion flow is more in the ion-diamagnetic direction than that of the impurities due to a negative diamagnetic correction to the impurity velocity from the pressure gradient term, with a dominant contribution from the impurity density gradient which increases strongly towards the plasma periphery. The somewhat different form of the predicted impurity velocities from the two theories in the outer half of the profile is due to different input density profiles. When calculating $v_\theta^{i,I}$ from Eqs. 1 and 2 the local outboard densities are used whereas and average of the measured density on the in- and outboard sides of the profile is used to evaluate $v_\theta^{i,I}$ from Eq. 3. This is solely a difference in the implementations, where in the first case the raw measurement data are used and in the latter case output data from TRANSP analysis of the discharges.

A breakdown of the contributions to the poloidal velocities driven by the temperature, pressure and toroidal rotation gradients expressed by the three terms of Eq. 3 is shown in Fig. 2. Consistent with the Kim theory, the poloidal flow of the bulk ions is predominantly driven by the temperature gradient, with a negligible contribution from the pressure gradient and none at all from the rotation shear. In the case of the impurities, the diamagnetic correction from the pressure gradient term is of similar magnitude to the temperature gradient driven flow, resulting in a net flow of ~ 3 km/s in the ion diamagnetic direction in the core, which is smaller than that of the bulk ions and of opposite sign in the periphery where the diamagnetic correction is larger.

In summary, both of the theories predict poloidal flow of the bulk ions in the diamagnetic direction of order $V_\theta^i \sim v_{thi}\rho_i / L_{T_i}$, which under the conditions prevailing on MAST is ≤ 5 km/s in magnitude. The $C^{6+}$ impurity flow is predicted to be more in the electron diamagnetic direction and typically smaller in magnitude than that of the bulk ions, even reversing direction in the plasma periphery. The alternative predictions of the theories of

Kim and Newton and Helander agree to within a factor of ~ 2 and flow shear is not expected to drive poloidal flow with $C^{6+}$ impurity ions in a deuterium plasma.

## 5 Charge-exchange velocity measurements

The charge-exchange recombination spectroscopy system on MAST [12] is equipped with a potential total of 288 spatial channels of which 224 can be viewed simultaneously through the high-throughput transmission grating spectrometer. The two heating beams are viewed by toroidal and poloidal arrays with 64 channels each and there are also 32 toroidal viewing background channels viewing away from the beams. As shown in Fig. 3, the poloidal views have two lenses per beam, each with 32 channels. viewing vertically downwards. The spectrometer can however only accommodate the 64 poloidal channels viewing one beam at a time. The radial coverage of the lenses is 0.9-1.2 m and 1.2-1.5 m, with a radial resolution $\Delta R \sim 1$ cm. One half of the fibres from each array view the beam and the other half the background light for the corresponding radial channels of the other array. Short in-vessel fibre bundles relay the light from the collection lenses to the viewport where relay optics couple the light onto external fibres of 400 μm diameter leading to the spectrometer. The in-vessel fibres are of 300 μm diameter and the collection lenses F/2.5 resulting in an overall étendu of ~ $10^{-8}$ $m^2$sr. The pixel size of the CCD detector is 12 μm and the dispersion of the spectrometer is 3.29 nm/mm, resulting in 0.0395 nm/pixel, and the measured instrumental width is 0.211 nm.

The most reliable CX measurements are obtained at the time of a fast cut-off of the NBI power, allowing subtraction of the background emission, measured during the 5 ms integration period following the cut-off, from the spectra measured during the preceding integration period. Reliable background subtraction is particularly important on MAST as the intensity of the ‘passive’ CX emission from the plasma edge due to charge exchange with excited neutrals is of comparable intensity to the ‘active’ CX emission because of the high edge neutral density. Fig. 4 shows an ‘active’ spectrum from the one of the poloidal channels for the integration period just before the NBI cut-off together with the background spectrum from the following integration period. Also shown is the spectrum resulting from subtraction of the background from the active spectrum, which, under the assumption that the ‘passive’ background emission remains constant over the

measurement period, should be solely due to the localised CX emission from the beam. The active spectrum has a peak intensity of ~ $5\times10^3$ counts, which is about twice that of the background spectrum. The error bars represent both the Poisson noise on the number of detected photons and the detector noise.

The active CX spectrum, which is a convolution of instrument function and the emission spectrum, is well represented by a Gaussian line profile with a FWHM of 0.397 nm, resulting in a measured ion temperature of 989±77 eV and poloidal velocity of 5.9±3.3 km/s in this example. Although the relative uncertainty is large in the poloidal velocity measurement, the absolute velocity is very small compared to the measured toroidal velocity of ≤ 180 km/s.

The MAST CX system does not have provision of opposing poloidal views, which would enable absolute velocities to be determined from the differential Doppler shift. Determination of absolute velocities relied instead on an absolute wavelength calibration of the CX spectrometer, performed for each discharge using a Cu I (529.252 nm, $j_i$-$j_k$ = 7/2-7/2) line emitted from a gas discharge lamp chosen because of its close proximity to the C VI (529.05 nm) line. Because the fiducial Cu I line differs in wavelength by only 0.2 nm from that of the C VI line, the dispersion of does not have to be known with high accuracy to determine the absolute wavelengths precisely. It is therefore considered to be a more accurate method than using measurements from a radial chord viewing passive C VI emission, which could potentially be contaminated by weak line emission from other impurities. During this operational period (2008) the poloidal views were set up to view the SS NBI beam line which was fitted with a JET type PINI ion source with a typical energy of 65 keV and an injected power of 1.8 MW.

**6 Comparison of measurements with neo-classical predictions:**

The data discussed in this section were from a 700 kA discharge in a balanced DND magnetic configuration with 1.8 MW of NBI heating at 65 keV injection energy. These discharges have an initial L-mode phase and then undergo a transition to largely ELM-free H-mode between 220 and 270 ms. The NBI power was cut off sharply at times during the L- or H-mode phases in several repeated discharges to obtain reliable CX profile measurements as discussed earlier. Profiles measured at 230 ms during the earlier

L-mode phase are shown in Fig. 5. The electron density profiles in L-mode are moderately peaked and the ion temperature equal to that of the electrons in the outer part of the plasma but somewhat higher in the core. The toroidal velocity profile is also peaked reaching 180 km/s in the centre. A change in the gradient of the toroidal velocity and ion temperature profiles inside about 1.25 m indicates the formation of an internal transport barrier (ITB) in the ion channel where the E×B flow shear, which is predominantly due to the shear in the toroidal flow, is sufficient to suppress the anomalous ion transport. The density of the $C^{6+}$ impurities is determined from the CX intensities using a neutral beam simulation to calculate the density of the beam neutrals [19]. As can be seen in Fig. 5 this peaks at about the same radial location as the foot of the ITB in the ion transport channel.

Over most of the profile, except in the very core where the uncertainties are large, the measured poloidal velocities of the $C^{6+}$ ions are of order 5±3 km/s in magnitude and consistent within the measurement uncertainties with the neo-classical prediction as calculated from Eq. (2). Note that there is a change in the sign of the carbon poloidal velocity at about 1.25 m in both the observations and in the neo-classical prediction. The predicted poloidal velocity of the bulk ions is in the ion diamagnetic direction peaking at about 5 km/s.

The separate contributions from the three terms in Eq. (2) to the predicted neo-classical $C^{6+}$ poloidal velocity are shown in Fig. 6. The first term represents the poloidal rotation driven by the bulk ion temperature gradient and the second and third terms are the contributions from the bulk and impurity ion pressure gradients respectively, i.e. due to their diamagnetic drifts. It can be seen that the inflection in the $C^{6+}$ velocity can be attributed both to the change in sign of the diamagnetic contribution to the $C^{6+}$ velocity and to a steepening of the bulk ion pressure gradient resulting in a larger, negative contribution from the second term at that location.

Profiles measured at 300 ms during the later H-mode phase are shown in Fig. 7. Note that in this discharge the transition to H-mode was earlier (220 ms) than in the discharge shown in Fig. 5. The electron density profile in this largely ELM-free H-mode phase is quite flat with a sharp gradient in the edge 'pedestal' region a few cm inside the separatrix. The $C^{6+}$ density also peaks at the top of the edge pedestal and then decays

further inside with an inflection at mid-radius, again peaking in the plasma core. This is an indication of weak accumulation of the carbon impurity. A sharp peaking of the profile of the soft x-ray emission (SXR) shows that high-Z impurities progressively accumulate in the plasma core during the H-mode phase. The toroidal velocity profile is also quite flat in this discharge, peaking at only 70 km/s. The reduction of core rotation compared to the earlier L-mode phase is because of the presence of a strong n=1 MHD mode which has started to slow down and lock by this late time in the discharge.

The observed $C^{6+}$ poloidal velocity is in the ion diamagnetic direction over most of the core plasma peaking at about 10 km/s, as is the case for the neo-classical prediction. The agreement between the observations and the neo-classical prediction is not always within the measurement uncertainties of ±3 km/s due to differences in the rotation profile shape. The change of direction of the $C^{6+}$ poloidal velocity observed in the L-mode data is not present in these H-mode discharges. This is both because the change in sign of the $C^{6+}$ density gradient and the steepening of the ion temperature gradient observed at mid-radius in the L-mode discharge shown in Fig. 5 are absent in the H-mode profiles shown in Fig. 7. This is an indication that the weak ITB present in L-mode is not present in the H-mode discharges.

In the edge pedestal region the observed poloidal velocities change sign to the electron diamagnetic direction. This is consistent with the presence of strong negative radial electric field in the pedestal region which is known to be important for the formation of the edge transport barrier (ETB) of H-mode plasmas [20]. The neo-classical prediction is not valid in this region because the scale length of the density gradient approaches that of the ion Larmor radius thus breaking the ordering of the theory.

In order to assess the reproducibility of these results data was obtained from several repeat discharges with the NBI cut-off at the same times during either the L- or H-mode phases. Profiles of the measured and predicted poloidal velocities of the $C^{6+}$ ions and the predicted poloidal velocities of the bulk ions are shown in Fig. 8 for three L-mode phases (left panels) and three H-mode phases (right panels). The profiles from each group of discharges are largely similar within the measurement uncertainties.

In the L-mode phases the $C^{6+}$ velocities increase from about zero at the plasma boundary to about 5 km/s at the mid-radius region at 1.25 m in agreement with the neo-classical prediction. Inside this location, the inflection to negative velocities of smaller magnitude is apparent in both the measurements and the neo-classical predictions in all three discharges. Inside ~ 1.1 m the measurement uncertainties increase to ~ ± 10 km due to the weaker active CX signal in this region. This is due both to the lower $C^{6+}$ density and the reduced beam density in the plasma core.

In the H-mode phases the observed and predicted $C^{6+}$ velocities are in the ion diamagnetic direction and somewhat higher than in the L-mode phases (≤ 10 km/s). The predicted bulk ion velocities are however smaller (≤ 5 km/s) due to the weaker bulk ion temperature gradient in H-mode in the mid-radius region. It is the resulting smaller negative contribution from the ion pressure gradient which results in the larger predicted $C^{6+}$ velocities which are consistent with the observations. As in the L-mode cases, the measurement uncertainties become large in the plasma core.

**7 Conclusions**

Poloidal velocities of impurity ions measured by means of CX spectroscopy are expected to be much less influenced by atomic physics corrections on MAST than on conventional, large tokamaks due to the lower toroidal field and ion temperature, these effects scaling as $\propto T_i B$. This facilitates comparison of the measurements with velocities predicted by theoretical models. Neo-classical theory predicts poloidal velocities of the bulk ions of order $V_\theta^i \sim v_{thi}\rho_i / L_{T_i}$ driven by the temperature gradient, which would typically be of magnitude ~ 5 km/s in the ion diamagnetic direction in MAST plasmas. As this scales as $\propto T_i / B$, the predicted neo-classical velocities on MAST and conventional tokamaks are comparable. Conditions are therefore much more favourable for comparing the measured poloidal flows on current spherical tokamaks like MAST than on conventional large tokamaks such as JET and DIII-D. The impurity ion velocity is not expected to be the same as that of the bulk ions because different flows perpendicular to the field are required to maintain radial force balance. Correcting for these diamagnetic flows typically results in impurity velocities less in the ion diamagnetic direction than that of the bulk ions. Calculation of the neo-classical velocities requires viscosity and inter-

species friction to be taken into account, and still more complete theories also account for the influence of toroidal rotation and the resulting poloidal redistribution of the heavy impurity density within a flux surface. Results presented here compare velocities predicted using expressions from two different neo-classical theories, one for a single impurity species in a bulk plasma of arbitrary collisionality and the other for a strongly rotating plasma with collisionless bulk ions which consider these effects respectively. The predicted velocities from these two theories agree to better than a factor two over the profiles and are of the expected magnitude $\leq 5$ km/s. Toroidal rotation is not expected to drive any poloidal flow when the charge/mass ratio of the impurities and bulk ions is equal and the main drive for the poloidal flow is the ion temperature gradient.

CX measurements from both poloidal and toroidal views are available on MAST with excellent radial resolution ~ 1 cm. The signal levels are also adequate to provide velocity and temperature measurements with reasonable accuracy. For measurement of typical toroidal velocities of ~ 200 km/s the uncertainties of ~ ±5 km/s are acceptable. The measured poloidal velocities are however much smaller and indeed of a similar magnitude to those predicted from neo-classical theory, i.e. ~ 5 km/s. A direct comparison relies on measuring the absolute velocity to a comparable or better accuracy, which in the case of the MAST CX system has to be performed using an absolute wavelength calibration using a suitable spectral line source. Using the most reliable estimate of this calibration the measured poloidal velocities are found to be consistent with the neo-classical predictions over most of the plasma radius in both L- and H-mode phases of MAST plasmas. Atomic physics corrections to the measurements are expected to be small ~ 1 km/s and would result in larger measured velocities in the ion diamagnetic direction. Accounting for these effects further improves the consistency between the measurements and the neo-classical predictions for the core plasma. In H-mode plasmas, higher poloidal velocities are measured in the electron-diamagnetic direction in the plasma periphery, consistent with the presence of a negative radial E-field in this region as usually observed in the H-mode pedestal region.

From the data presented here, there is no evidence for poloidal velocities of the bulk or impurity ions in MAST plasmas significantly exceeding those expected according to neo-classical theory in standard L- and H-mode plasmas. Although these plasmas are not

specifically produced to generate ITBs, in MAST as in other STs with strong tangential NBI heating, the very high sheared toroidal rotation in the core plasma does suppress the anomalous ion thermal transport to a level comparable to the neo-classical rate in the mid-radius region. It could therefore be argued that there is usually an ion ITB present in many MAST discharges. The observed rates of poloidal rotation in these plasmas are however consistent with the predictions of standard neo-classical theory and a strong turbulent drive for poloidal rotation seems not to be present. This is somewhat contradictory to observation of poloidal velocities far in excess of neo-classical rates in the presence of ITBs in the conventional tokamaks DIII-D [6] and JET [7, 11]. In contrast, preliminary poloidal velocity measurements on the NSTX ST device are also consistent with the predictions of neo-classical theory [9]. It is suggested that perhaps at low aspect ratio the neo-classical damping of poloidal rotation is stronger than at large aspect ratio and can overcome any turbulent drive, which may be responsible for the observations of poloidal velocities in excess of neo-classical levels in the presence of ITBs in conventional tokamaks.

**Acknowledgement**

*This work was supported by the Engineering and Physical Sciences Research Council and by the European Communities under the contract of Association between EURATOM and UKAEA. The views and opinions expressed herein do not necessarily reflect those of the European Commission.*

## References


[1] S. Newton, *'Collisional Transport in a Low Collisionality Plasma with strong Rotation'*, Ph.D. thesis, University of Bristol, 2007.

[2] S. Newton and P. Helander, Phys. Plasmas, **13** (2006) 102505.

[3] Y. B. Kim, P. H. Diamond and R. J. Groebner, Phys. Fluids B, **3** 8 (1991) 2050–2059.

[4] P. Hirshman and D. J. Sigmar, Nucl. Fusion, **21** (1981) 1079.

[5] P. H. Diamond, Y. B. Kim, Phys. Fluids B, 3 (1991) 1626.

[6] W. M. Solomon, K. H. Burrell, R. Andre et al., Phys. Plasmas, **13** (2006) 056116.

[7] K. Crombé, Y. Andrew, M. Brix et al., Phys. Rev. Lett., **95** 15 (2005) 155003.

[8] R. E. Bell, F. M. Levington, S. H. Baha, E. J. Synakowski and M. C. Zarnstorff, Phys. Rev. Lett. **81** 7 (1998) 1429–1432.

[9] R. E. Bell. R. Feder, 50$^{th}$ DPP Meeting of the APS, Dallas, Texas, Bulletin of the American Physical Society 2008, NP6.119.

[10] G. M. Staebler, R. E. Waltz, J. E. Kinsey et al., Nucl. Fusion, **41** (2001) 891–899.

[11] T. Tala, Y. Andrew, K. Crombé et al., Nucl. Fusion, **47** (2007) 1012-1023.

[12] N. J. Conway, P. G. Carolan, J. McCone, et al., Rev. Sci. Inst., 77 (2006) 10F131.

[13] R. E. Bell and E. J. Synakowski, Ann. Isr. Phys. Soc., **547** (2000) 39.

[14] H. P. Summers, Atomic Data and Analysis Structure, JET Report JET-IR(94)-06.

[15] A. R. Field, G. Fussmann, J. V. Hofmann, Nucl. Fusion, **32** (1992) 1191–1208.

[16] M. J. Walsh, Rev. Sci. Inst., **74** (2003) 1663-1666.

[17] A. Patel, Rev. Sci. Inst., **75** (2004) 4944-4950

[18] L. L. Lao et al., Nucl. Fusion, **30** (1990) 1035.

[19] M. R. Turnyanskij, *'Experimental Investigation of Ion Behaviour on the START Tokamak'*, PhD thesis, University of Essex, Colchester (1998).

[20] P. Gohil, K. H. Burrell, E. J. Doyle et al., Nucl. Fusion, **34** (1994) 1057-1068.

***Figures:***

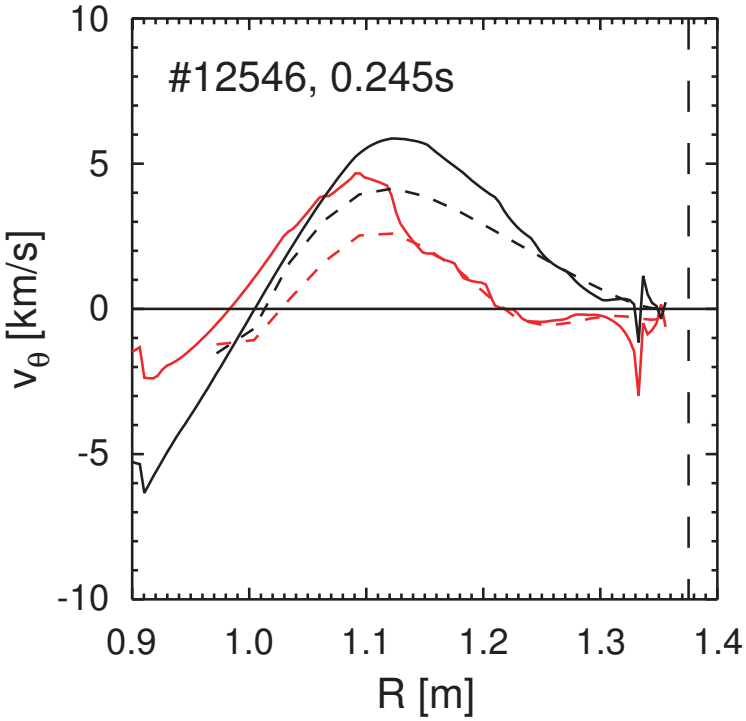


*Fig. 1: Neo-classical poloidal velocities of the bulk ions $V_\theta^i$ (black) and the $C^{6+}$ impurity ions $V_\theta^I$ (red) calculated according to the theories of Kim [1] (solid) and Newton [2] (dashed) for discharge #12546 at the time of NBI cut-off at 245 ms. The separatrix location is indicated by the vertical dashed line.*

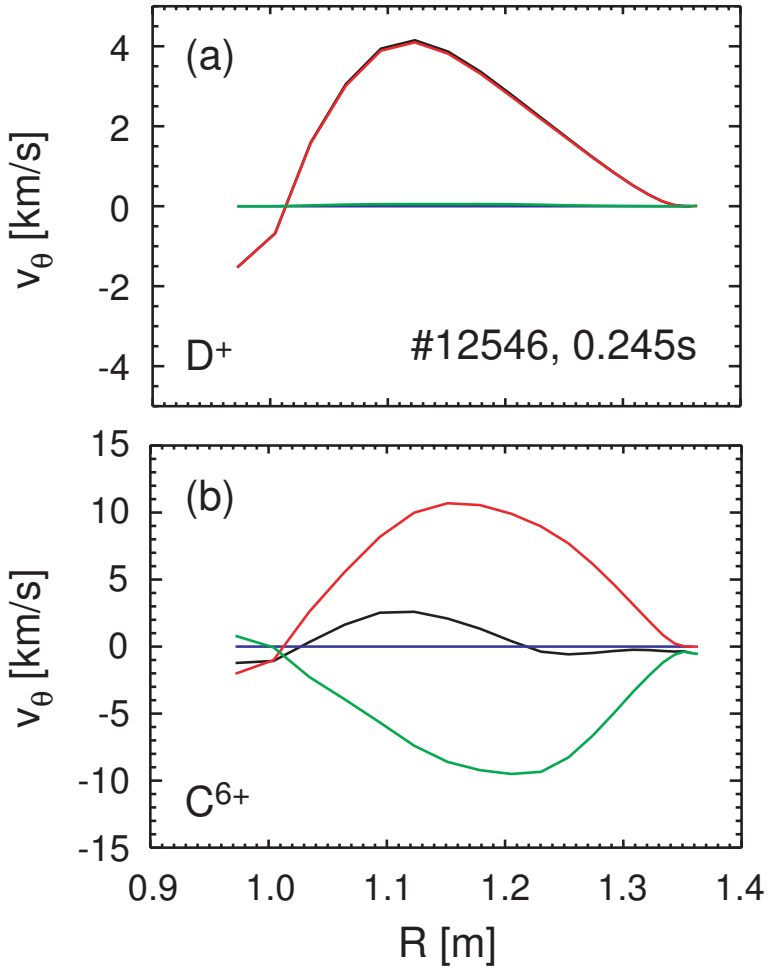


*Fig. 2 Neo-classical poloidal velocities of (a) bulk ions and (b) $C^{6+}$ impurity ions calculated from the theory of Newton [2]. The net $v_\theta$ (black) and the separate contributions driven by the temperature gradient (red), the pressure gradient (green) and the velocity shear (blue) are shown. Note the different y-axis ranges in Figs. (a) and (b).*

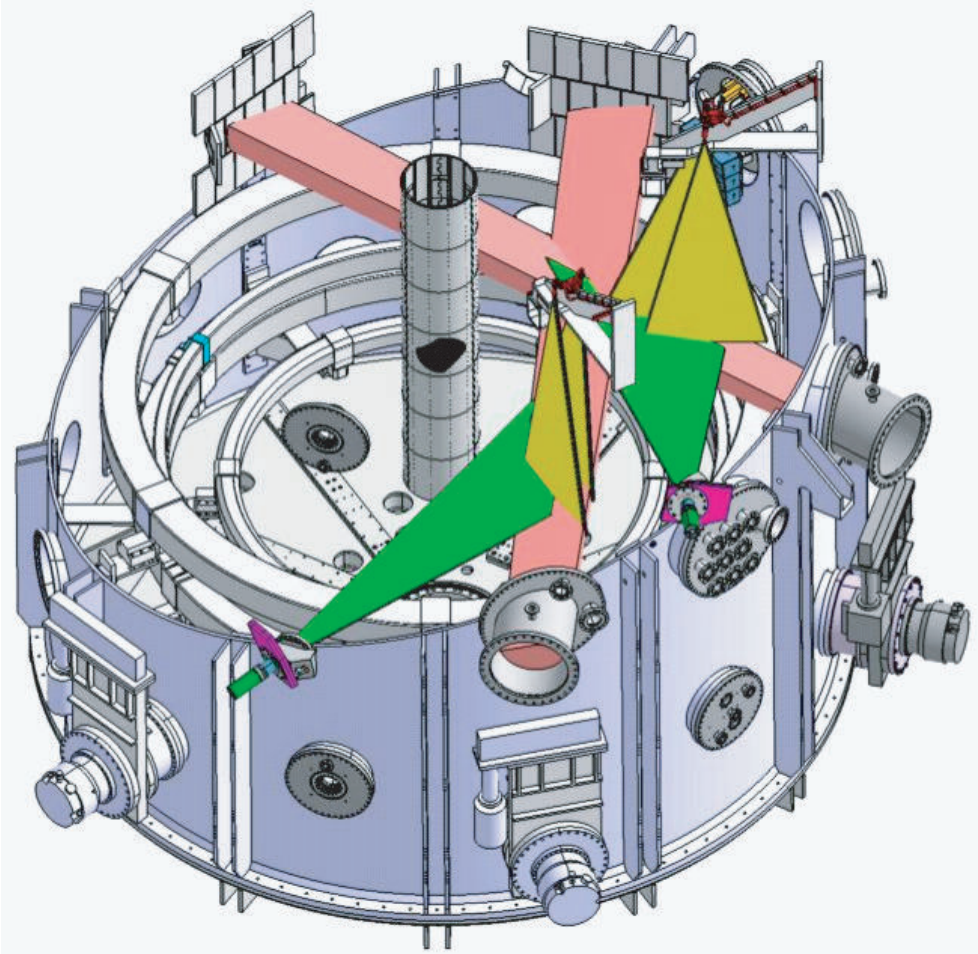

*Fig. 3 Schematic drawing showing the viewing geometry of the CXRS system on MAST. The two NBI beams are shown in mauve, the extent of the tangentially oriented toroidal views in green and the vertically oriented poloidal views in orange.*

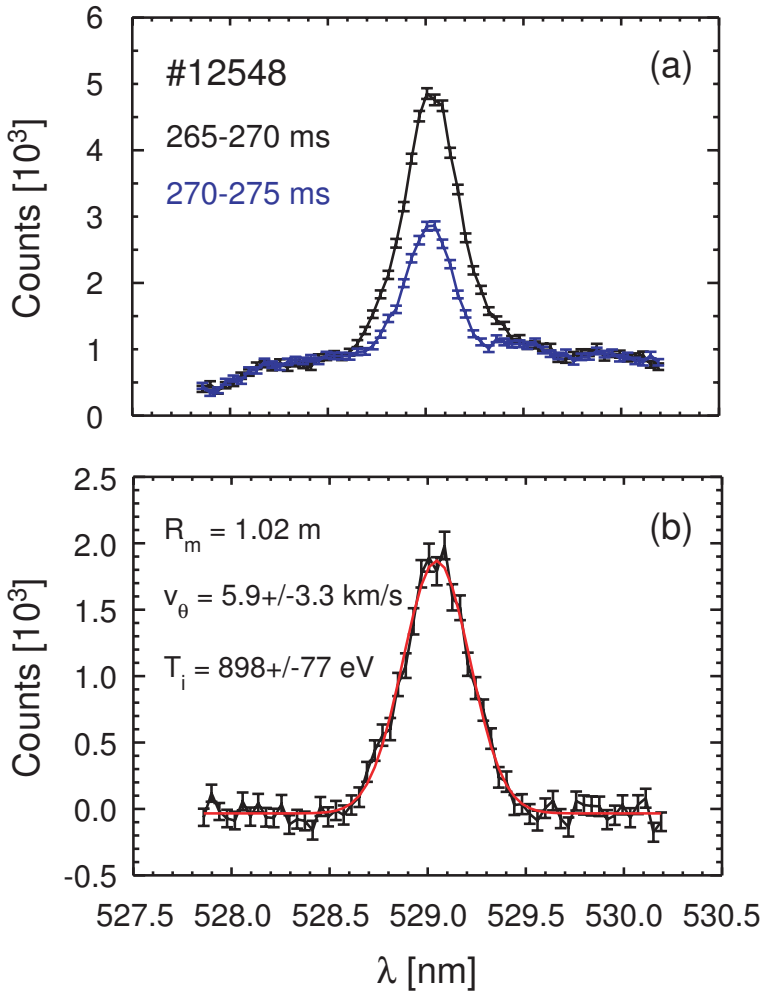


*Fig. 4 Example of spectral data showing: (a) raw CVI (529.05 nm) spectra from the integration period just before and after the NBI cut-off from one poloidal channel of the CXRS spectrometer and (b) the 'active' CX signal resulting from subtraction of the spectra in (a) together with a fitted Gaussian line profile.*

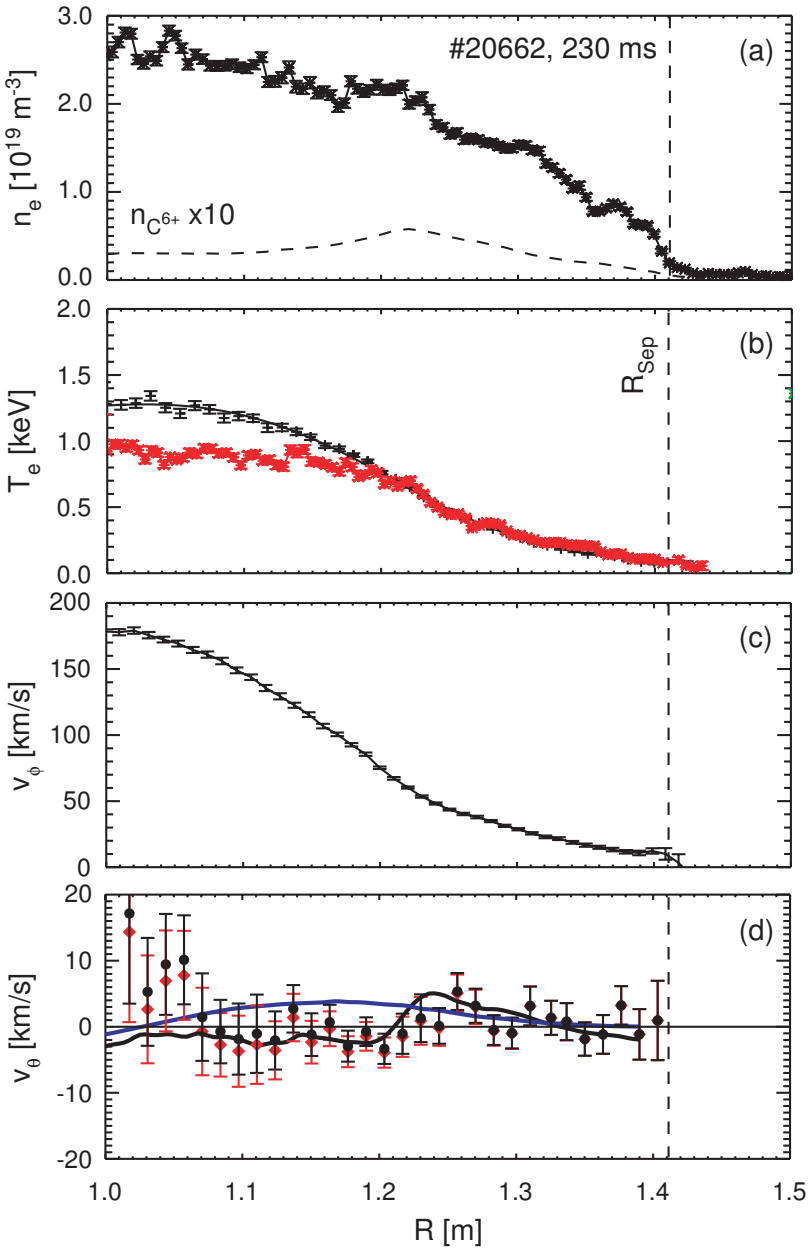


*Fig. 5: Profiles measured during the early L-mode phase of a 700 kA discharge with 1.8 MW of NBI heating: (a) $n_e$ from ruby TS system and $C^{6+}$ density determined from CXRS intensities; (b) $T_e$ from ruby TS system and ion temperature of $C^{6+}$ ions from CXRS system; (c) toroidal velocity profile; and (d) poloidal velocities of $C^{6+}$ ions directly from observed Doppler shift (♦) and after correction for pseudo velocities (●) with the predicted neo-classical $C^{6+}$ velocity (black line) and bulk ion velocity (blue line), where positive values are in the ion diamagnetic direction. The separatrix location is indicated by the dashed vertical line.*

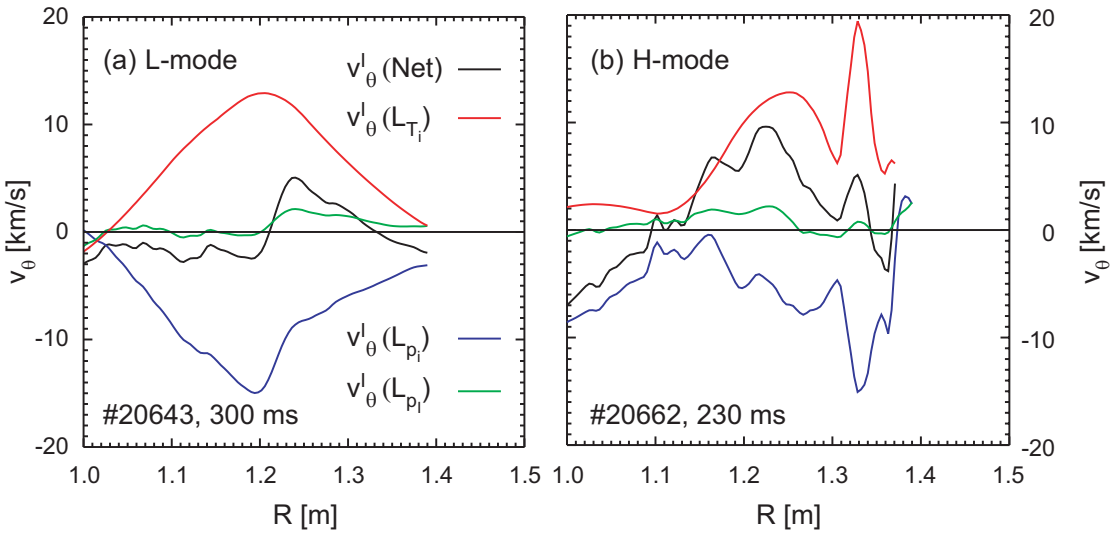


*Fig. 6 Profiles of the neo-classical poloidal velocity of the $C^{6+}$ impurities calculated from Eq. (2) (black) for (a) the same L-mode phase as shown in Fig.5 and (b) for the H-mode phase as shown in Fig. 7. Also shown are the separate contributions from the bulk ion temperature gradient (red), the bulk pressure gradient (blue) and the impurity pressure gradient (green) representing the three terms of Eq. 2.*

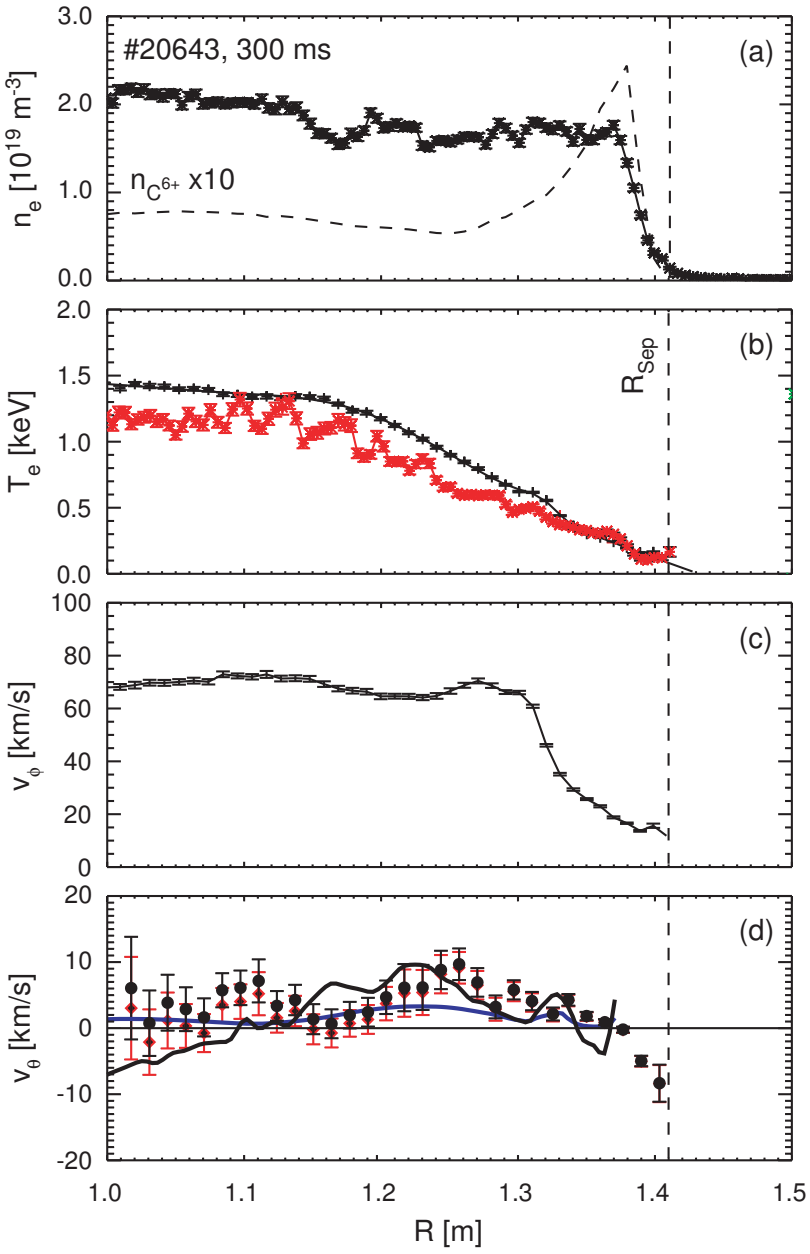


*Fig. 7: Profiles measured during the later ELM-free H-mode phase of a 700 kA discharge with 1.8 MW of NBI heating as specified in Fig. 5.*

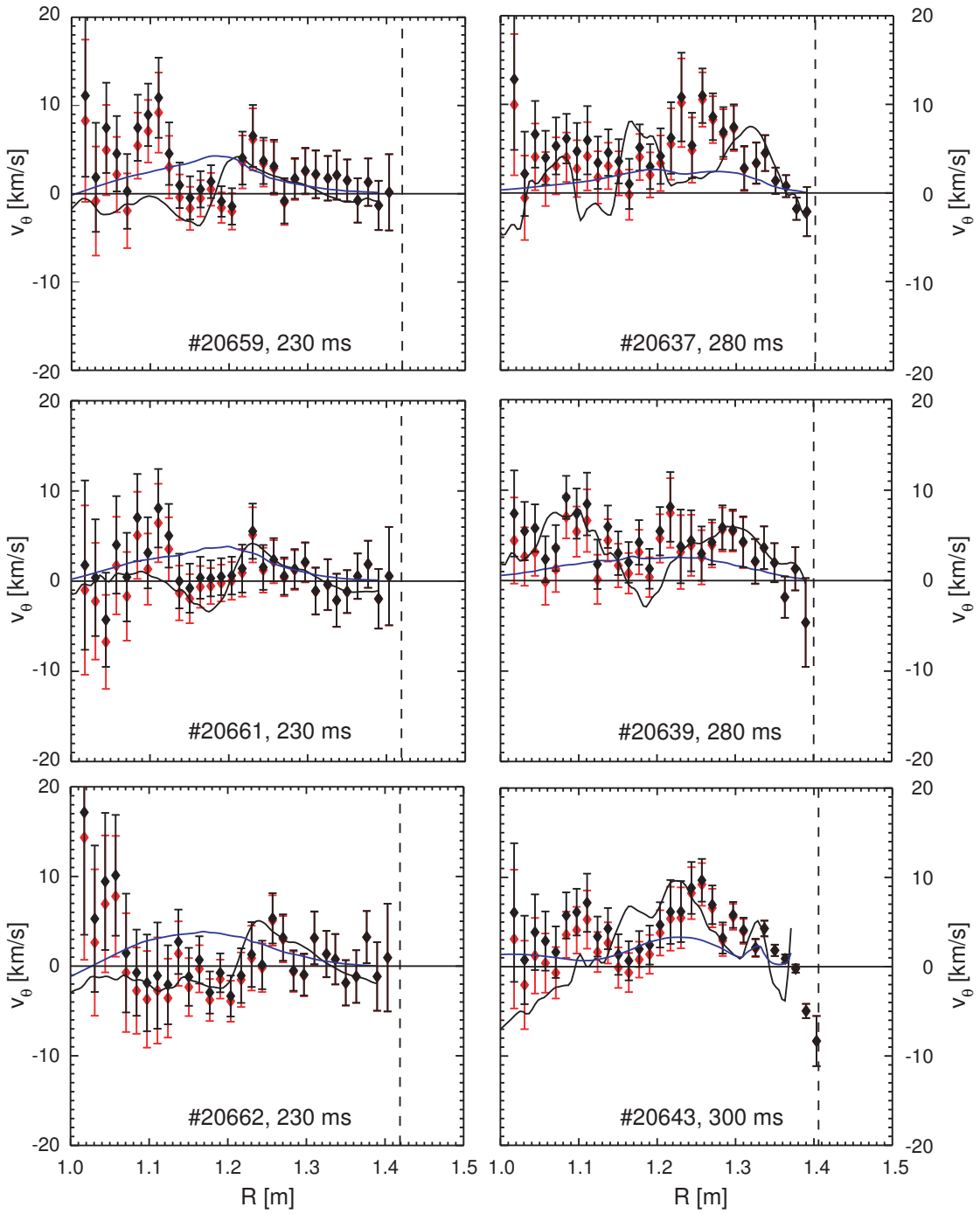


*Fig. 8: Comparison of poloidal velocity profiles in six similar discharges during L-mode (left) and ELM-free H-mode phases (right) showing velocities of $C^{6+}$ ions directly from observed Doppler shift (♦) and after correction for pseudo velocities (♦) with the predicted neo-classical $C^{6+}$ velocity (black line) and bulk ion velocity (blue line), where positive values are in the ion diamagnetic direction.*